Magnetodielectric coupling in Mn_3O_4

R. Tackett and G. Lawes
Department of Physics and Astronomy, Wayne State University, Detroit, Michigan 48201, USA

B. C. Melot, M. Grossman, E. S. Toberer, and R. Seshadri
Materials Department and Materials Research Laboratory, University of California, Santa Barbara, California 93106, USA
(Received 26 March 2007; revised manuscript received 17 May 2007; published 6 July 2007)

We have investigated the dielectric anomalies associated with spin-ordering transitions in the tetragonal spinel Mn_3O_4 using thermodynamic, magnetic, and dielectric measurements. We find that two of the three magnetic ordering transitions in Mn_3O_4 lead to decreases in the temperature-dependent dielectric constant at zero applied field. Applying a magnetic field to the polycrystalline sample leaves these two dielectric anomalies practically unchanged, but leads to an increase in the dielectric constant at the intermediate spin-ordering transition. We discuss possible origins for this magnetodielectric behavior in terms of spin-phonon coupling. Band structure calculations suggest that in its ferrimagnetic state, Mn_3O_4 corresponds to a semiconductor with no orbital degeneracy due to strong Jahn-Teller distortion.

DOI: 10.1103/PhysRevB.76.024409 PACS number(s): 75.50.Gg, 75.47.Lx, 77.22.−d, 71.15.Mb

I. INTRODUCTION

Magnetodielectrics can be described as materials in which magnetic ordering produces dielectric anomalies or, alternately, materials in which the low-frequency dielectric constant is sensitive to an external magnetic field.[1] These materials have been studied for several decades, but the recent surge in activity in studying multiferroics[2,3] has prompted renewed interest in understanding the origins of the spin-charge coupling in these systems. While multiferroics are also magnetodielectric, the converse is frequently not true. Nevertheless, characterizing the shifts in the dielectric constant induced by magnetic ordering offers crucial insights into possible spin-charge coupling mechanisms. Additionally, the recognition that substantial magnetodielectric coupling often arises in systems with noncollinear magnetic structures[4–6] offers the possibility that dielectric spectroscopy may be a simple yet powerful tool for identifying phase transitions among complex magnetic structures.

Magnetodielectric coupling has been investigated both theoretically and experimentally in a wide range of materials, including $BaMnF_4$,[7–10] Cr_2BeO_4,[11] $LiCoPO_4$,[12] and $Gd_2(MoO_4)_3$.[13] Studies of $BaMnF_4$ proved to be particularly illuminating, as substituting 1% of the Mn sites with Co changes the magnetic point group, allowing a detailed study of the symmetry of the magnetodielectric coupling.[9] Extending these earlier studies, several new magnetodielectrics have been identified and investigated more recently, including $SeCuO_3$,[4] $EuTiO_3$,[14] $BiMnO_3$,[15] $CoCr_2O_4$,[16,17] and $TmFeO_3$.[18] There has also been considerable interest in investigating magnetocapacitive coupling in multiferroics.[2,3]

Several models have been proposed for explaining the observed dependence of the low-frequency dielectric constant on spin structure and external magnetic field. The simplest of these postulates a dielectric response which varies as the square of the net magnetization.[14,15] These models fail to account for the large dielectric shifts observed at antiferromagnetic transitions, which can be qualitatively understood by considering a coupling between the dielectric constant and the q-dependent spin-spin correlation function[4] or nearest-neighbor magnetic energies.[10] There have also been numerous models suggested for possible microscopic mechanisms giving rise to the observed magnetodielectric couplings. It has been suggested that coupling between long-wavelength polar phonon modes and spin structure could shift the dielectric constant in $BaMnF_4$ (Ref. 7); this mechanism has been reexamined to explain magnetodielectric coupling in $SeCuO_3$.[4] Single-ion effects[19] and a spin-current model[5] have also been proposed as possible mechanisms. It has recently been recognized that magnetoresistive contributions in inhomogeneous systems can also give rise to magnetocapacitive effects.[20,21] This result highlights the importance of distinguishing extrinsic magnetocapitance from intrinsic spin-charge coupling.

In the following, we discuss the synthesis and characterization of the magnetodielectric spinel Mn_3O_4 whose structure is displayed in Fig. 1. The magnetic structure of Mn_3O_4 was investigated in the 1960s,[22] and the dielectric properties have been studies more recently by Suzuki *et al.*[23] This later research found that Mn_3O_4 displays a sharp drop in the dielectric constant at the ferrimagnetic T_C=42 K. This feature was attributed to the orbital degrees of freedom in this system. Since Mn_3O_4 is known to exhibit several complex low-temperature spin states,[24–27] we conducted more detailed measurements of the dielectric constant at each of the magnetic transitions in order to elucidate how specific spin structures yield different magnetocapacitive couplings. At the onset of long-range magnetic order in Mn_3O_4 below 42 K, the A-site Mn^{2+} spins order ferromagnetically along [010], while the B-site Mn^{3+} spins order along [001]. Below 39 K these B-site spins order in a spiral structure with an incommensurate propagation vector along [010], and at 33 K these Mn^{3+} ions exhibit a more complex order with the 16 ions in the magnetic unit cell having a net moment antiparallel to the Mn^{2+} spin direction.[24]

II. EXPERIMENTAL AND COMPUTATIONAL DETAILS

Well-sintered, brown pellets of Mn_3O_4 were prepared from the oxalate $MnC_2O_4 \cdot 2H_2O$ by decomposing at 650 °C

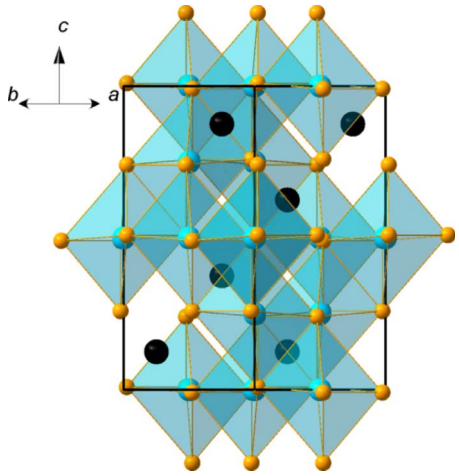

FIG. 1. (Color online) Crystal structure of the tetragonal compound Mn_3O_4 derived from the cubic spinel through a strong Jahn-Teller distortion. The black spheres are tetrahedrally coordinated Mn^{2+} on the *A* site and the cyan spheres are the octahedrally coordinated Mn^{3+} on the *B* site. Orange spheres are O.

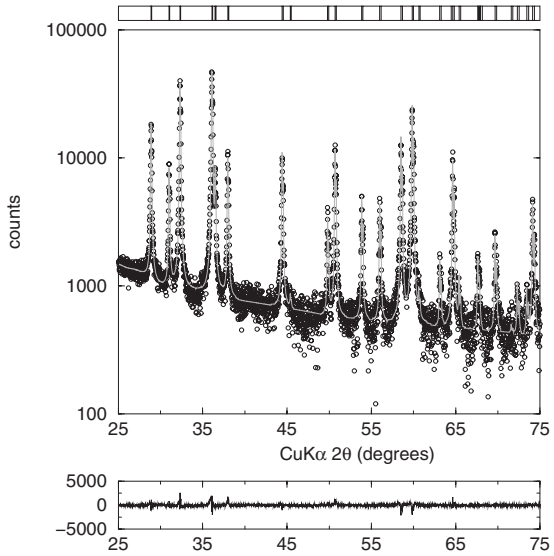

FIG. 2. X-ray diffraction Rietveld analysis of Mn_3O_4 showing data as small circles and fits as gray lines. The vertical lines at the top of the figure indicate expected peak positions. Rietveld analysis gave $a=5.7631_1$ Å and $c=9.4712_3$ Å. The position of the O atom was determined to be $(0,0.4700_5,0.2563_3)$. Subscripts indicate experimental uncertainties in the last decimal place.

for 1 h, pelletizing, and heating to 1200 °C for 12 h, following which the pellets were rapidly cooled to room temperature. Rapid cooling was required in order to avoid producing Mn_2O_3 as an impurity phase. X-ray diffraction patterns were obtained using Cu $K\alpha$ radiation on a Philips X'PERT MPD diffractometer operated at 45 kV and 40 mA, and subject to Rietveld refinement using the XND Rietveld code.[28]

The dc magnetization of Mn_3O_4 was measured a Quantum Design superconducting quantum interference device (SQUID) magnetometer as a function of temperature and field. We measured the specific heat and ac susceptibility using standard options on a Quantum Design PPMS, which was also used to regulate the temperature and magnetic field for dielectric measurements. For specific heat measurements, approximately 30 mg of the powder sample was cold pressed into a solid pellet, which was found to have a small internal thermal time constant. To measure the dielectric properties, we pressed a circular pellet from approximately 50 mg of sample, then fashioned parallel-plate electrodes using conducting silver epoxy. The dielectric measurements were done at an excitation frequency of 30 kHz with a drive of 1 V. There was no significant frequency or bias dependence to the measurements.

The electronic structure of Mn_3O_4 was calculated using density functional methods. For these calculations, we used the linear muffin tin orbital (LMTO) method within the generalized gradient approximation (GGA), as implemented in the STUTTGART TB-LMTO-ASA program.[29] Starting structures for LMTO calculations were obtained from experimental Rietveld refinements. Two hundred and sixty-two irreducible *k* points were employed within the irreducible part of the Brillouin zone.

III. RESULTS AND DISCUSSION

Mn_3O_4 is a tetragonally distorted spinel, as illustrated in Fig. 1, with space group $I4_1/amd$ (No. 141). The polycrystalline samples used in this study were monophasic as revealed by x-ray diffraction Rietveld analysis shown in Fig. 2. In this structure, Mn^{2+} ions are located at the tetrahedral site at $(0,\frac{1}{4},\frac{7}{8})$ and Mn^{3+} ions at the octahedral site $(0,\frac{1}{2},\frac{1}{2})$. O is at the general position $(0,y,z)$, More structural details are provided in the caption of Fig. 1. Suzuki *et al.*[23] have suggested that the e_g orbital at the Mn^{3+} site is partially occupied, leading to an orbital degree of freedom. However, it is known that on cooling Mn_3O_4 undergoes a transition from a cubic spinel to Jahn-Teller distorted tetragonal structure at 1433 K.[30] As a consequence of this Jahn-Teller structural distortion on Mn^{3+}, the electronic structure of tetragonal Mn_3O_4 as calculated here using density functional theory, and previously using Hartree-Fock theory[31] suggests no orbital degeneracy.

The LMTO-GGA densities of states calculated for collinear ferrimagnetic Mn_3O_4, and projected onto the different Mn atoms and onto O, are displayed in the panels of Fig. 3. The system is characterized by large exchange splitting: near 4 eV on the tetrahedral *A* site (occupied by Mn^{2+}) and near 3 eV on the octahedral *B* site (occupied by Mn^{3+}). Both sites are completely spin polarized, with the crystal field configurations as indicated in the caption of the figure. The Jahn-Teller distortion on the octahedral *B* site manifests clearly in the majority-spin channel, which is seen to comprise filled t_{2g}^3 states centered around −2 eV, separated from a filled $d_{z^2}^1$ state just below $E=0$. The empty majority $d_{x^2-y^2}$ states are found centered near 1 eV. The minority Mn *d* states at the *B* site are all empty and found starting at 0 eV. The crystal field splitting at the *B* site is of the order of 4 eV. O *p* states are found a little below the filled Mn *d* states, which is not surprising given the position of Mn in the middle of the first transition-metal series. As would be expected for a fully

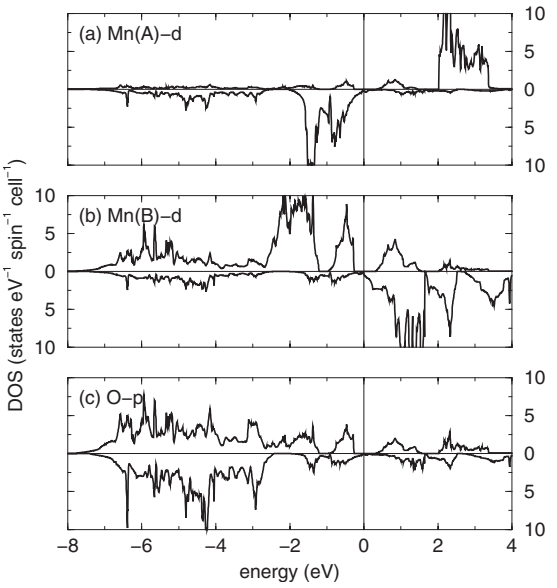

FIG. 3. Projected LMTO-GGA densities of states of semiconducting, Néel-ferrimagnetic Mn_3O_4 plotted in the two spin directions. (a) Tetrahedral d^5 Mn^{2+} on the A site showing filled minority e and t_2 states and empty majority e and t_2 states. (b) Octahedral Mn^{3+} on the B site with a Jahn-Teller distortion resulting in a gap within filled and empty e_g states: majority $d^1_{z^2}$ is separated from majority $d^0_{x^2-y^2}$. All minority states are empty. (c) The O p states. The origin on the energy axis is the top of the valence band.

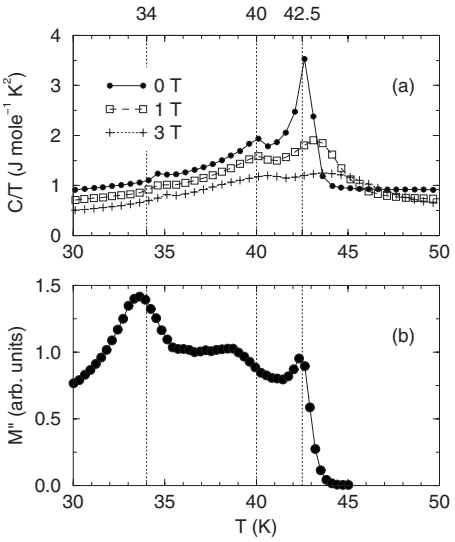

FIG. 4. (a) Mn_3O_4 ac susceptibility measured at $\omega/2\pi = 10$ kHz and zero field. (b) Mn_3O_4 specific heat measured at $H=0$, $H=1$ T, and $H=3$ T. For clarity, the $H=0$ T and $H=1$ T data have been offset by 0.2 and 0.1 J mol^{-1} K^2, respectively.

spin-polarized ferrimagnet, the calculated magnetic moment per Mn_3O_4 formula unit is precisely $3\mu_B$, corresponding to eight spins from two octahedral Mn^{3+} ions, compensated for by five spins from the tetrahedral Mn^{2+} ion.

In order to identify the numerous magnetic transitions in Mn_3O_4 we first measured the specific heat capacity of this sample, both at zero magnetic field and under the application of a field. These results are shown in panel (a) of Fig. 4. There are three distinct peaks in the heat capacity at $H=0$, corresponding to magnetic phase transitions at roughly $T=34$ K, $T=40$ K, and $T=42$ K. Approximating the lattice background to the specific heat as a constant 0.5 J mol^{-1} K^2 over the the small temperature range of the peak, we find a total spin entropy of approximately $1.2k_B/Mn_3O_4$. This is somewhat smaller than previously reported values,[25] but consistent with the suggestion that substantial geometrical frustration reduces the entropy change from the full value expected for complete spin order $\approx 5k_B/Mn_3O_4$. These three peaks in the Mn_3O_4 specific heat correspond to the development of complex spin structures investigated previously by neutron diffraction measurements.[24] Applying a magnetic field produces substantial broadening in the 42-K peak, but does not significantly shift the transition temperatures, at least for fields up to $H=3$ T.

We also see distinct features corresponding to these magnetic transitions in Mn_3O_4 in ac susceptibility measurements. The imaginary component of the complex susceptibility measured at 10 kHz is plotted in panel (b) of Fig. 4. The three peaks in the magnetic loss signal correspond to the three magnetic phase transitions observed the specific heat data. There is a substantial increase in the magnetic loss at the onset of long-range magnetic order at 42 K, which remains high through the additional magnetic phase transitions at 40 K and 34 K. Small features are also observed in the real component of the complex magnetization (not shown), but these these anomalies are more difficult to discern against the large signal from the 42 K transition. The upper panel of Fig. 5 plots the zero-field-cooled (ZFC) and field-cooled (FC) temperature-dependent dc magnetization under a measuring field of 1000 Oe and the temperature-dependent magnetic hysteresis loops. The transition to long-range order

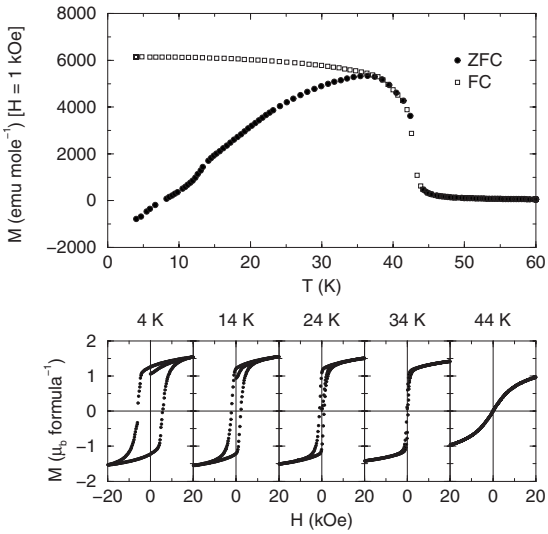

FIG. 5. (a) Zero-field-cooled (ZFC) and field-cooled (FC) magnetization curves for Mn_3O_4 measured in a field of 1000 Oe. (b) Magnetic hysteresis loops measured at temperatures from $T=4$ K (far left) to $T=44$ K (far right).

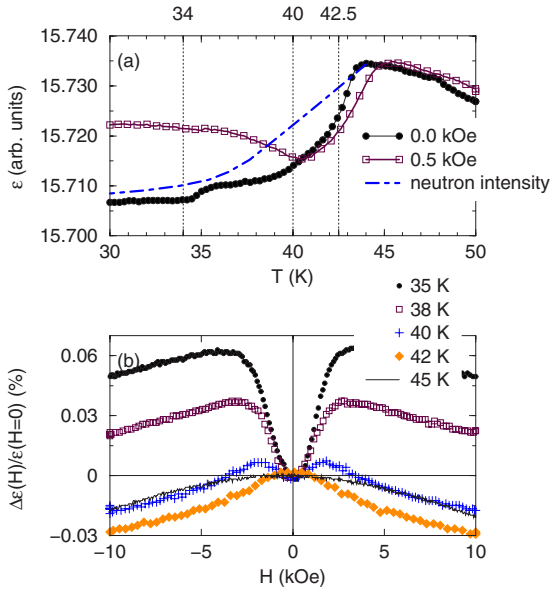

FIG. 6. (Color online) (a) Temperature-dependent dielectric constant of Mn_3O_4 at $H=0$ (solid circles) and $H=5$ kOe (open squares). The dashed line is the scaled neutron intensity of the (120) reflection taken from Ref. 24. (b) Magnetic field dependence of the dielectric constant of Mn_3O_4 at different temperatures.

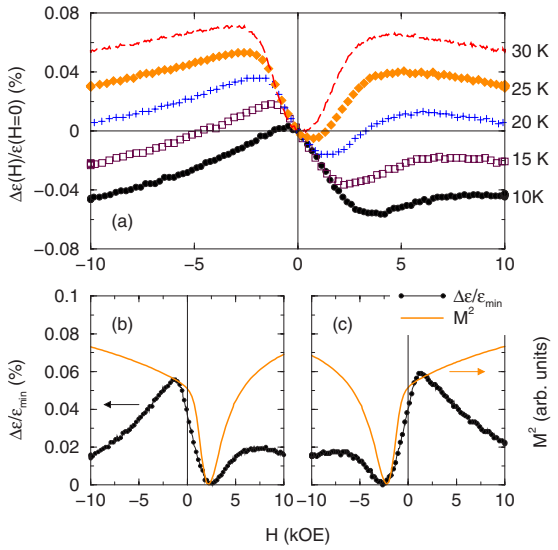

FIG. 7. (Color online) (a) Percentage change in Mn_3O_4 dielectric constant (relative to $H=0$) as a function of increasing magnetic field at fixed temperatures of 30 K, 25 K, 15 K, and 10 K (upper trace to lower). (b) Solid curve: percentage change in Mn_3O_4 dielectric constant (relative to the minimum value). Dashed line: square of the net magnetization. Both are measured as a function of increasing magnetic field measured at 15 K. (c) Relative change and net magnetization measured as a function of decreasing magnetic field at 15 K.

at 42 K is clearly visible, as is a small anomaly at $T=15$ K in the ZFC curve, but the two additional magnetic phase transitions at $T=34$ K and $T=40$ K give no signal. $M(H)$ loops plotted in the lower panel of Fig. 5 show a net saturation magnetization corresponding to a moment of $\approx 1.5\mu_B$/f.u., with significant coercivity developing only at temperatures below 34 K.

The temperature-dependent dielectric constant of Mn_3O_4 close to these magnetic ordering transitions is shown in Fig. 6(a). At zero applied magnetic field, we see a sharp decrease in the dielectric constant at 42 K, coincident with the onset of long-range magnetic order in Mn_3O_4. The dielectric constant decreases by approximately 0.2%, consistent with the magnitude of the drop observed previously in Mn_3O_4.[23] In addition to the large drop in dielectric constant at 42 K, we observe a much smaller, but still distinct, negative shift of 0.015% in the dielectric constant at the 34 K magnetic transition. A hint of such behavior is also visible in previous studies of Mn_3O_4.[23] While both the 42-K and 34-K magnetic transitions in Mn_3O_4 lead to clear dielectric anomalies at zero field, there is no suggestion of any magnetodielectric coupling associated with the 40-K transition. However, the application of a modest magnetic field substantially alters the dielectric response of Mn_3O_4. The negative magnetodielectric shifts associated with the 42-K and 34-K transitions remain relatively unchanged, but the 40-K magnetic transition now produces a significant *increase* in dielectric constant.

In order to probe the effects of an applied magnetic field on the dielectric response of Mn_3O_4 we measured the dielectric constant at fixed temperature as a function of applied field. These data are plotted in Fig. 6(b). In the paramagnetic phase, there is a very slight decrease in dielectric constant with magnetic field. Just below the onset of long-range magnetic order, the shift in dielectric constant with applied field remains negative, but with a change in curvature. However, the development of the spiral magnetic structure below 40 K leads to positive magnetodielectric shifts at low magnetic fields, followed by smaller decreases at higher fields. The increase in dielectric constant saturates at approximately 0.06% in a field of 3 kOe.

We extended our measurements on the magnetic field dependence of the dielectric constant to lower temperatures, below the 34-K transition. As shown in Fig. 5, Mn_3O_4 develops magnetic hysteresis at low temperatures, with the coercive field reaching approximately 5 kOe by $T=10$ K. Figure 7(a) plots the relative shift in dielectric constant as a function of *increasing* magnetic field, measured at fixed temperatures. At $T=30$ K, there is a slight asymmetry in the curve; this asymmetry increases substantially as the temperature is reduced. We attribute this asymmetry to magnetic hysteresis in Mn_3O_4 at lower temperatures. Figures 7(b) and 7(c) plot the change in dielectric constant relative to the minimum value, together with the square of the magnetization at $T=15$ K, separately for increasing and decreasing magnetic fields. While the relative change in dielectric constant does not simply follow the square of the magnetization, the minimum dielectric constant does occur at (approximately) the coercive field, where $M=0$. As we will discuss in the following, we believe the dielectric shift in Mn_3O_4 is not determined by the net magnetization, but rather a more complex spin-spin correlation function for the magnetically ordered phase.

IV. DISCUSSION

Several factors have been suggested to contribute to magnetization-induced changes in dielectric constant, including spin-phonon coupling,[4,32] electronic structure,[33] orbital degrees of freedom,[23] and magnetoresistive effects.[20] Electromagnon scattering has also been proposed to explain the increase in dielectric constant observed at certain magnetic transitions in multiferroics.[34,35]

Previous studies on Mn_3O_4 have suggested that orbital degrees of freedom play an important role in the observed magnetodielectric coupling.[23] This proposal adequately explains the differences observed in the magnetodielectric coupling among Mn_3O_4, $MnCr_2O_4$, and MnV_2O_4, but it is unclear how orbital effects could give rise to the multiple dielectric anomalies observed in Fig. 6. Because the Mn_3O_4 samples used in this investigation are polycrystalline, it is particularly important to consider the magnetoresistive Maxwell-Wagner mechanism proposed by Catalan[20] as a possible origin for magnetocapacitance. We do not believe that the dielectric anomalies we observe in Mn_3O_4 at magnetic phase transitions are associated with magnetoresistive effects between the grain boundaries and interiors. Over the frequency range investigated ($\omega/2\pi=3$ kHz to 1 MHz), the Mn_3O_4 dielectric constant shows no relaxational effects, which are generically expected for Maxwell-Wagner capacitors with a $1/RC$ time constant.[20] Furthermore, the dielectric shift depends strongly only magnetic field only below the 40 K transition, as shown in Fig. 6. This argues against simple magnetoresistance as being the origin for the magnetodielectric coupling, which is very clearly present at the highest temperature transition. Finally, we do not find any evidence for secondary phases in the XRD shown in Fig. 2.

In the following, we will consider the suggestion that spin-structure-induced shifts in phonon frequencies can produce changes in the dielectric constant through the Lydanne-Sachs-Teller relation.[4,7] In this framework, the polar-optic-phonon frequencies, hence dielectric constant, are coupled to the spin-spin correlation function for the magnetic structure, so the dielectric constant should vary with the neutron peak intensity. The onset of long-range order in Mn_3O_4, which produces a significant drop in the dielectric constant, is associated with the growth of the (120) neutron peak intensity.[24] We have extracted the intensity of the (120) peak from Ref. 24 and plotted this as a dashed line in Fig. 6 after correcting for a small difference in transition temperature. While the drop in dielectric constant in Mn_3O_4 is somewhat steeper than the increase in neutron intensity, the dielectric shift approximately follows the intensity in the (120) peak and, in particular, both level off below 35 K.

While the qualitative agreement between the (120) neutron intensity and drop in the Mn_3O_4 dielectric constant below 42 K are consistent with the spin-phonon model for magnetodielectric coupling, the detailed mechanism remains unclear. As a first step in developing a microscopic model it is necessary to identify which specific phonon modes couple to the complex spin structure. The deformation produced by the octahedral Jahn-Teller Mn^{3+} ions gives rise to the tetragonal distortion to $I4_1/amd$ symmetry in Mn_3O_4. This distortion leads to ten allowed Raman active modes $\Gamma=2A_{1g}+3B_{1g}+B_{2g}+4E_g$, rather than the five modes in cubic spinels with $Fd\bar{3}m$ symmetry.[36,37] A total of ten of the phonon modes are infrared active;[36] shifts in these polar modes will change the Mn_3O_4 dielectric constant. Experimentally, only five Raman modes are observed,[36] including a large-amplitude A_{1g} mode at 660 cm^{-1} attributed to the motion of oxygen ions inside the MnO_6 octahedra and associated with the cooperative Jahn-Teller distortion.[37] As magnetodielectric coupling is often associated with noncollinear spin structures,[16] this large-A_{1g} Raman peak may provide a suitable signal to investigate possible spin-phonon coupling involving the B-site Mn^{3+} ions. Any evidence for significant spin-phonon coupling in Mn_3O_4 (not limited to coupling to polar phonons) would provide important guidance for establishing the microscopic origins of the magnetodielectric coupling.

As the (120) neutron scattering intensity varies smoothly below 42 K,[24] some additional spin-phonon coupling must be responsible for the dielectric anomaly observed at 35 K in zero field. Below 40 K, an additional neutron scattering reflection is observed at $(1,1+\tau,0)$. The propagation vector $q=1-\tau$ increases monotonically with decreasing temperature. This peak locks in at $q=1$ at the 34-K magnetic transition, which also produces a sharp increase in intensity.[24] We suppose that this low-temperature magnetic structure also couples to an optic-phonon mode in Mn_3O_4, giving rise to the dielectric shift observed below 34 K. Between 34 K and 40 K, τ is nonzero and temperature dependent and the magnetic structure is incommensurate with the lattice structure. The spin-phonon coupling coefficient is predicted to vary with the overlap between the q-dependent spin structure and phonon mode.[4] The incompatibility between spin and lattice structure could lead to a varying coupling coefficient, which averages to zero and gives no net magnetodielectric coupling. Only when the spin structure locks in at $q=1$ at 34 K does the spin-phonon coupling constant become nonzero. We point out that incommensurate magnetic structures can lead to very dielectric anomalies associated with transitions into ferroelectrically ordered phases.[38–40] This is distinctly different from our observations of Mn_3O_4, which seem to suggest that incommensurate magnetic structures do not produce sizable dielectric anomalies.

It is rather more difficult to motivate the positive shift in dielectric constant below 40 K in an applied magnetic field and positive magnetocapacitance in this temperature range (see Fig. 6). One possibility is that even a modest magnetic field, below 3 kOe, is sufficient to lock in some commensurate value for the propagation vector q of the (110) structure, leading to nonzero magnetodielectric coupling. Because the low-temperature dielectric constant shows hysteretic effects compatible with the magnetic hysteresis curves shown in Fig. 5, this (110) spin structure may also be expected to exhibit hysteresis. Alternatively, some additional mechanism for magnetodielectric coupling beyond the spin-phonon model considered here may be relevant. Additional studies of the magnetic field dependence of the Mn_3O_4 dielectric constant on single-crystal samples may be required to clarify the origins of the positive magnetocapacitance observed between 34 K and 40 K at low fields.

In summary, we have investigated the dielectric properties of Mn_3O_4 in detail and found evidence for magnetodielectric coupling associated with specific magnetic structures. An incommensurate magnetic transition in Mn_3O_4 produces no dielectric anomaly at zero magnetic field, but applying modest fields produces an increase in dielectric constant at this transition. These magnetodielectric features can be qualitatively understood using a spin-phonon coupling model, although a more detailed understanding of the specific phonons involved in the coupling would be necessary to compare theory and experiment in detail.

ACKNOWLEDGMENTS

Work at Wayne State University was supported by the Donors of the American Chemical Society Petroleum Research Fund (Grant No. PRF 46160-G10) and the Institute for Manufacturing Research. Work at UCSB was supported by the National Science Foundation through Career Award No. DMR 0449354 and by NSF Chemical Bonding Center Grant No. CHE 0434567. We also profited from facilities supported by NSF MRSEC Program No. DMR 0520415 at UCSB.

[1] R. E. Newnham, *Properties of Materials: Anisotropy, Symmetry, Structure* (Oxford University Press, New York, 2005).
[2] N. A. Spaldin and M. Fiebig, Science **309**, 391 (2005).
[3] W. Eerenstein, N. D. Mathur, and J. F. Scott, Nature (London) **442**, 759 (2006).
[4] G. Lawes, A. P. Ramirez, C. M. Varma, and M. A. Subramanian, Phys. Rev. Lett. **91**, 257208 (2003).
[5] H. Katsura, N. Nagaosa, and A. V. Balatsky, Phys. Rev. Lett. **95**, 057205 (2005).
[6] M. Mostovoy, Phys. Rev. Lett. **96**, 067601 (2006).
[7] G. A. Samara and P. M. Richards, Phys. Rev. B **14**, 5073 (1976).
[8] D. L. Fox and J. F. Scott, J. Phys. C **10**, C11 (1977).
[9] D. L. Fox, D. R. Tilley, J. F. Scott, and H. J. Guggenheim, Phys. Rev. B **21**, 2926 (1979).
[10] J. F. Scott, Phys. Rev. B **16**, 2329 (1977).
[11] R. E. Newnham, J. J. Kramer, W. A. Schulze, and L. E. Cross, J. Appl. Phys. **49**, 6088 (1978).
[12] I. Kornev, M. Bichurin, J.-P. Rivera, S. Gentil, H. Schmid, A. G. M. Jansen, and P. Wyder, Phys. Rev. B **62**, 12247 (2000).
[13] H. Wiegelmann, B. K. Ponomarev, J. Van Tol, A. G. M. Jansen, P. Wyder, and B. S. Red'kin, Ferroelectrics **183**, 195 (1996).
[14] T. Katsufuji and H. Takagi, Phys. Rev. B **64**, 054415 (2001).
[15] T. Kimura, S. Kawamoto, I. Yamada, M. Azuma, M. Takano, and Y. Tokura, Phys. Rev. B **67**, 180401(R) (2003).
[16] G. Lawes, B. Melot, K. Page, C. Ederer, M. A. Hayward, Th. Proffen, and R. Seshadri, Phys. Rev. B **74**, 024413 (2006).
[17] Y. Yamasaki, S. Miyasaka, Y. Kaneko, J.-P. He, T. Arima, and Y. Tokura, Phys. Rev. Lett. **96**, 207204 (2006).
[18] R. Muralidharan, T.-H. Jang, C.-H. Yang, Y. H. Jeong, and T. Y. Koo, Appl. Phys. Lett. **90**, 012506 (2007).
[19] M. Mercier, E. F. Bertaut, G. Quezel, and P. Bauer, Solid State Commun. **7**, 149 (1969).
[20] G. Catalan, Appl. Phys. Lett. **88**, 102902 (2006).
[21] G. Lawes, R. Tackett, O. Masala, B. Adhikary, R. Naik, and R. Seshadri, Appl. Phys. Lett. **88**, 242903 (2006).
[22] K. Dwight and N. Menyuk, Phys. Rev. **119**, 1470 (1960).
[23] T. Suzuki, K. Adachi, and T. Katsufuji, J. Phys.: Conf. Ser. **31**, 235 (2006).
[24] G. B. Jensen and O. V. Nielson, J. Phys. C **7**, 409 (1974).
[25] A. Kuriki, Y. Moritomo, S. Xu, K. Ohoyama, K. Kato, and A. Nakamura, J. Phys. Soc. Jpn. **72**, 458 (2003).
[26] J. M. Hastings and L. M Corliss, Phys. Rev. **126**, 556 (1962).
[27] K. Tomiyasu, J. Fukunaga, and H. Suzuki, Phys. Rev. B **70**, 214434 (2004).
[28] J.-F. Bérar and G. Baldinozzi, Commiss. Powder Diffract. Newslett. **20**, 3 (1998).
[29] O. K. Andersen, Phys. Rev. B **12**, 3060 (1975); O. Jepsen and O. K. Andersen, Z. Phys. B: Condens. Matter **97**, 35 (1995).
[30] H. J. van Hook and M. L. Keith, Am. Mineral. **43**, 69 (1958).
[31] A. Chartier, P. D'Arco, R. Dovesi, and V. R. Saunders, Phys. Rev. B **60**, 14042 (1999).
[32] A. B. Harris, T. Yildirim, A. Aharony, and O. Entin-Wohlman, Phys. Rev. B **73**, 184433 (2006).
[33] R. C. Rai, J. Cao, S. Brown, J. L. Musfeldt, D. Kasinathan, D. J. Singh, G. Lawes, N. Rogado, R. J. Cava, and X. Wei, Phys. Rev. B **74**, 235101 (2006).
[34] A. Pimenov, A. A. Mukhin, V. Y. Ivanon, V. D. Travkin, A. Balbashov, and A. Loidl, Nat. Phys. **2**, 97 (2006).
[35] A. B. Sushkov, R. V. Aguilar, S. Park, S-W. Cheong, and H. D. Drew, Phys. Rev. Lett. **98**, 027202 (2007).
[36] H. D. Lutz, B. Muller, and H. J. Steiner, J. Solid State Chem. **90**, 54 (1991).
[37] L. Malavasi, P. Galinetto, M. Mozzati, C. Azzoni, and G. Flor, Phys. Chem. Chem. Phys. **4**, 3876 (2002).
[38] G. Lawes, A. B. Harris, T. Kimura, N. Rogado, R. J. Cava, A. Aharony, O. Entin-Wohlman, T. Yildrim, M. Kenzelmann, C. Broholm, and A. P. Ramirez, Phys. Rev. Lett. **95**, 087205 (2005).
[39] T. Kimura, T. Goto, H. Shintani, K. Ishizaka, T. Arima, and Y. Tokura, Nature (London) **425**, 55 (2003).
[40] M. Kenzelmann, A. B. Harris, S. Jonas, C. Broholm, J. Schefer, S. B. Kim, C. L. Zhang, S.-W. Cheong, O. P. Vajk, and J. W. Lynn, Phys. Rev. Lett. **95**, 087206 (2005).